Progress In Electromagnetics Research Letters, Vol. 84, 59–65, 2019

A Compact Multiband MIMO Antenna for IEEE 802.11 a/b/g/n Applications

Wenying Wu, Ruixing Zhi, Yingjian Chen, Han Li, Yanhua Tan, and Gui Liu*

Abstract—A compact multiband multiple-input-multiple-output (MIMO) antenna for WLAN applications is presented in this paper. The proposed MIMO antenna consists of two symmetric monopole radiating elements designed to operate over 2.45, 5.2, and 5.8 GHz bands. The isolation is enhanced by using several techniques such as parasitic elements and defected ground structure. The measured $S_{11} < -10$ dB is obtained over 2.36–2.68 GHz and 4.81–5.95 GHz, which can cover IEEE 802.11 a/b/g/n frequency bands (2.4–2.4835 GHz, 5.15–5.35 GHz, and 5.725–5.875 GHz). The measured isolation values S_{21} are less than -24 dB and -27 dB over the lower and higher frequency bands, respectively. The envelope correlation coefficient (ECC) of the proposed antenna is less than 0.027 and 0.005 over the lower and higher operating bands, respectively. The overall size of the proposed antenna is $50 \times 30 \times 1.59\,\text{mm}^3$. The proposed antenna is a good candidate for IEEE 802.11 a/b/g/n applications.

1. INTRODUCTION

WITH the advancement of wireless communication technology, there is an increasing demand for wireless communication devices with high data rate and large channel capacity. Multiple-input-multiple-output (MIMO) antennas are capable of inherently mitigating the effects of multipath, resulting in improved link reliability, channel capacity, gain, bandwidth, and diversity performance. More and more attentions have been focused on the design of the MIMO antennas.

In recent years, the trend in modern wireless system is miniaturization. A variety of radiation structures have been proposed to reduce antenna size. However, compact size results in strong electromagnetic coupling and weak isolation between antenna elements. The isolation performance of MIMO antennas can be enhanced by loading SRRs [1, 2], neutralizing line [3–5], Y-shape isolator element [6], a wide slot and a pair of narrow slots [7], meandering-line resonator [8], bent T-shaped resonator [9], and an elliptical slot and a rectangular parasitic strip [10]. There are also some novel structures such as reconfigurable MIMO antenna [11] and simple decoupling structure [12].

In this letter, we propose a novel and compact MIMO antenna that offers multiband operation in the bands of IEEE 802.11 a/b/g/n. The monopole radiating element includes two L-shaped stubs and an E-shaped strip loaded with two rectangle stubs. Two antenna elements are placed in parallel to maximize the spatial separation which provides diverse patterns. The parasitic element (PE) and defected ground structure (DGS) on the ground plane result in a suppression of surface wave propagation, which can reduce mutual coupling between the radiating elements and improve antenna efficiency.

Received 11 March 2019, Accepted 30 April 2019, Scheduled 21 May 2019

* Corresponding author: Gui Liu (iitgliu2@gmail.com).

The authors are with the College of Mathematics, Physics & Electronic Information Engineering, Wenzhou University, Wenzhou, Zhejiang 325035, China.

2. ANTENNA GEOMETRY AND DESIGN

The structure of the proposed antenna is shown in Figure 1. The proposed MIMO antenna was fabricated on an FR-4 substrate with $\varepsilon_r = 4.4$, $\tan\delta = 0.02$, and the thickness of 1.59 mm. Two symmetric monopole radiating elements and feed lines are printed on the top side of the substrate while the defected ground plane is on the bottom side. The widths of the feed lines are 3 mm, and they are connected to two L-shaped stubs through an E-shaped strip for impedance matching. In this work, the two monopoles are located symmetrically at the left and right sides of the substrate, and the distance between the two feed lines is 25 mm.

The radiation elements consist of two L-shaped stubs, an inverted E-shaped strip, and a rectangular strip. The value of length L_3 can be used to tune the resonance frequency bandwidth. Figure 2 shows the simulated reflection coefficients of the proposed antenna for various L_3 lengths. It can be seen that the length of L_3 affects the lower frequency band while the higher frequency remains almost unchanged. The optimum value of length L_3 is 3 mm, and the -10 dB impedance bandwidth of the lower frequency band is 170 MHz (2.38 to 2.55 GHz) which can cover 2.4–2.4835 GHz.

The higher resonant frequency band can be tuned by adjusting the value of length L_7, as shown in Figure 3. The value of length L_7 can be optimized for the higher frequency band while the lower frequency band remains almost unchanged. The optimized value of L_7 is 3 mm, and the -10 dB

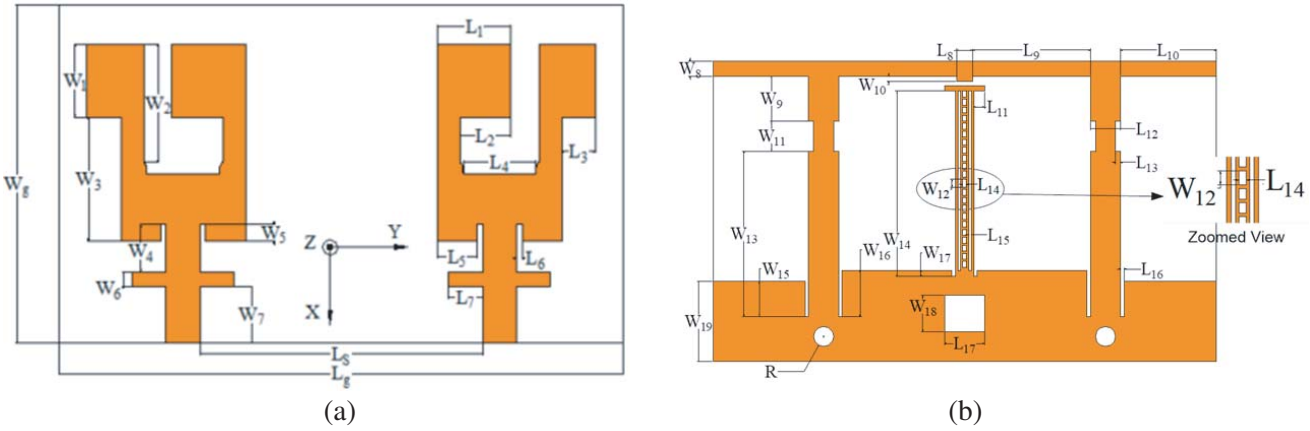

Figure 1. Configuration of the proposed MIMO antenna. (a) Top view. (b) Bottom view.

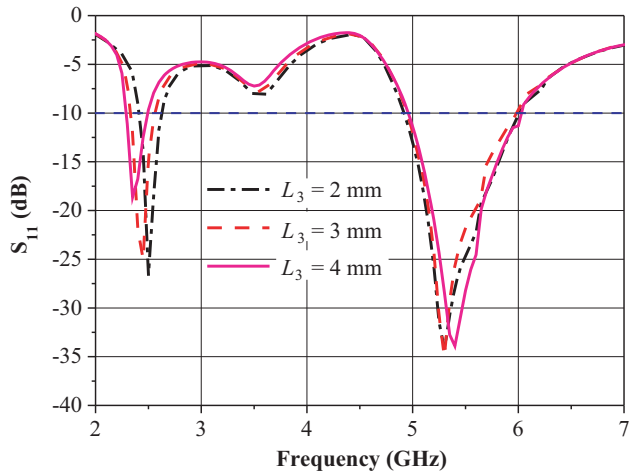

Figure 2. Simulated reflection coefficients of the proposed antenna with different values of L_3.

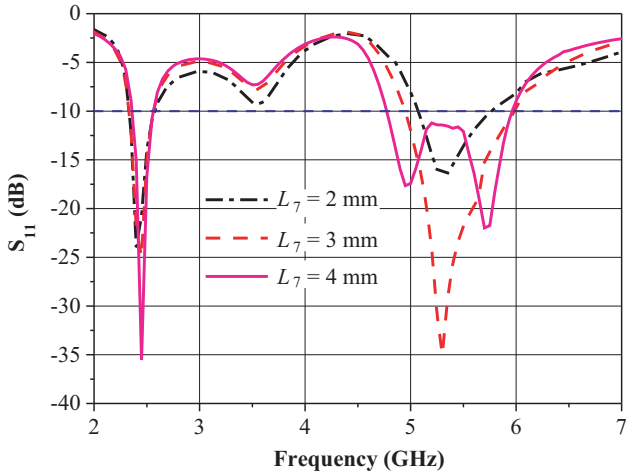

Figure 3. Simulated reflection coefficients of the proposed antenna with different values of L_7.

impedance bandwidth of the higher frequency band is 1003 MHz (4.95 to 5.98 GHz) which can cover both 5.15–5.35 GHz and 5.725–5.875 GHz frequency bands.

In this design, the isolation between two antenna elements has been enhanced by introducing parasitic elements and defected ground structure. The parasitic elements consist of two short T-shaped strips and a π-shaped strip. Two 17.9 mm long slits and twenty two 0.4 mm $\times$ 0.6 mm rectangle slots are cut from the short T-shaped strips on the ground plane to reduce mutual coupling and improve impedance matching. Simulated isolation values of the proposed antenna with different structures are shown in Figure 4. It can be observed that the isolation performance is improved obviously at the lower operating band for the MIMO antennas with the short T-shaped strip and π-shaped strip.

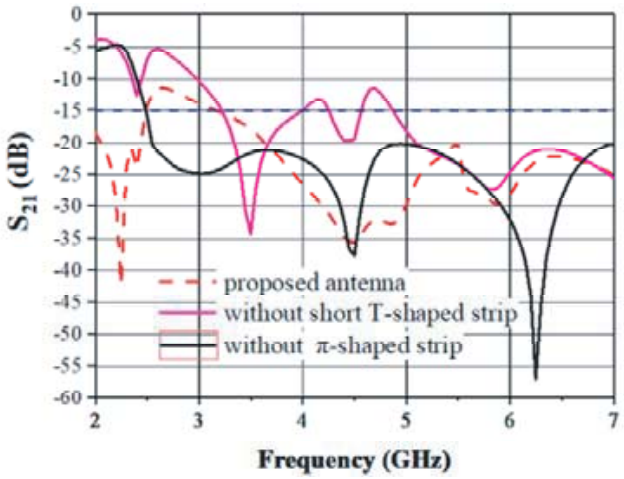

Figure 4. Simulated isolation of the proposed antenna with different structures.

Table 1. Parameters of the proposed antenna (in millimeters).

L_g	W_g	W_1	W_2	W_3	W_4	W_5	W_6	W_7	W_8	W_9	W_{10}	W_{11}	W_{12}
50	30	6.5	10.5	11	4.2	1.5	1.3	5	1.3	4.5	0.5	3	0.6
W_{13}	W_{14}	W_{15}	W_{16}	W_{17}	W_{18}	W_{19}	L_1	L_2	L_3	L_4	L_5	L_6	L_7
16.5	18.5	3.5	4.6	0.6	3.6	8	6.5	4.5	3	6.4	3.5	0.5	3
L_8	L_9	L_{10}	L_{11}	L_{12}	L_{13}	L_{14}	L_{15}	L_{16}	L_{17}	R	L_S		
1.6	11.7	9.5	1.1	3	0.5	0.4	0.25	0.35	4	1	25		

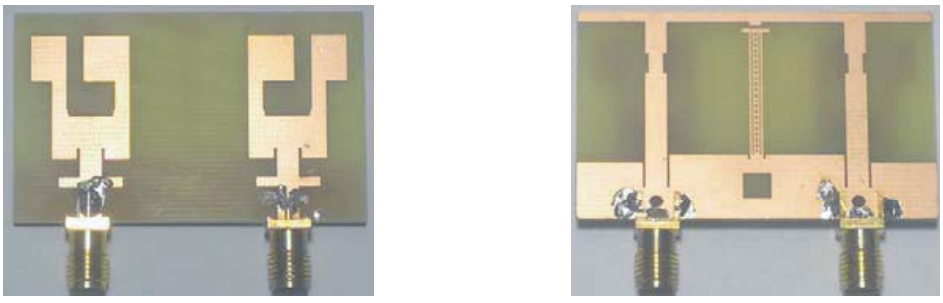

(a) (b)

Figure 5. Photograph of the fabricated prototype. (a) Top view. (b) Bottom view.

3. RESULTS AND DISCUSSION

The dimensions of the proposed antenna after optimization are listed in Table 1. Photographs of the fabricated prototype are shown in Figure 5.

As shown in Figure 6, the measured impedance bandwidths for −10 dB reflection coefficients are 320 MHz (2.36–2.68 GHz) and 1180 MHz (4.81–5.99 GHz), which can cover IEEE 802.11 a/b/g/n frequency bands (2.4–2.5 GHz, 5.15–5.35 GHz and 5.725–5.875 GHz).

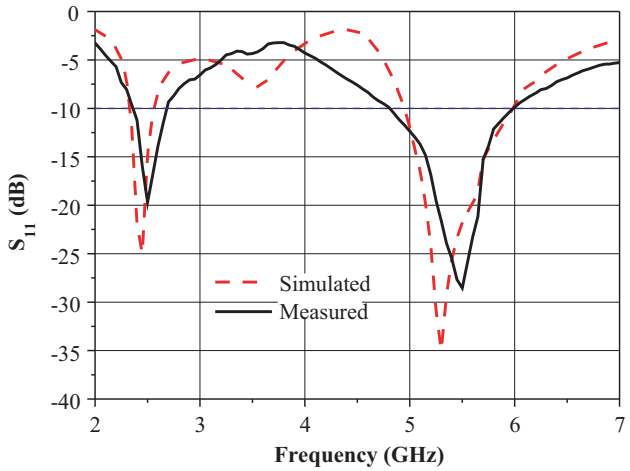

Figure 6. Simulated and measured reflection coefficients of the proposed antenna.

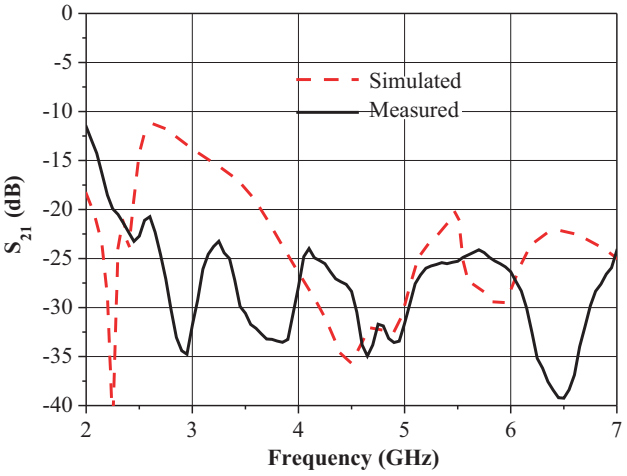

Figure 7. Simulated and measured isolation of the proposed antenna.

The measured S_{21} at three desired frequency bands (2.4–2.5 GHz, 5.15–5.35 GHz, and 5.725–5.875 GHz) are lower than −20 dB, as depicted in Figure 7. There is a deviation of S_{21} between simulated and measured ones due to fabrication errors and losses in soldered SMA at the lower frequency band.

The measured peak gain and efficiency are demonstrated in Figure 8. The measured average gains at the lower and higher frequency bands are approximately −0.3 dBi and 2.4 dBi, respectively. The average radiation efficiencies at the lower and higher frequency bands are 32.89% (from 29.34% to 36.37%) and 63.80% (from 61.90% to 65.70%), respectively. The loss of the FR-4 substrate and the cable used in measurement contribute to low gain and efficiency at the lower frequency band.

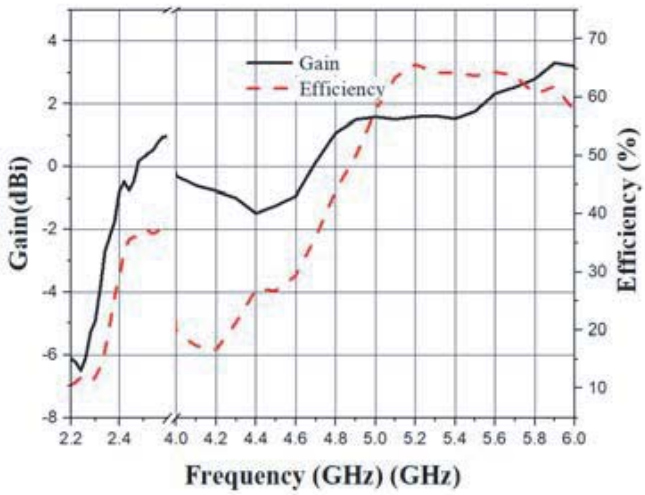

Figure 8. Measured peak gain and efficiency.

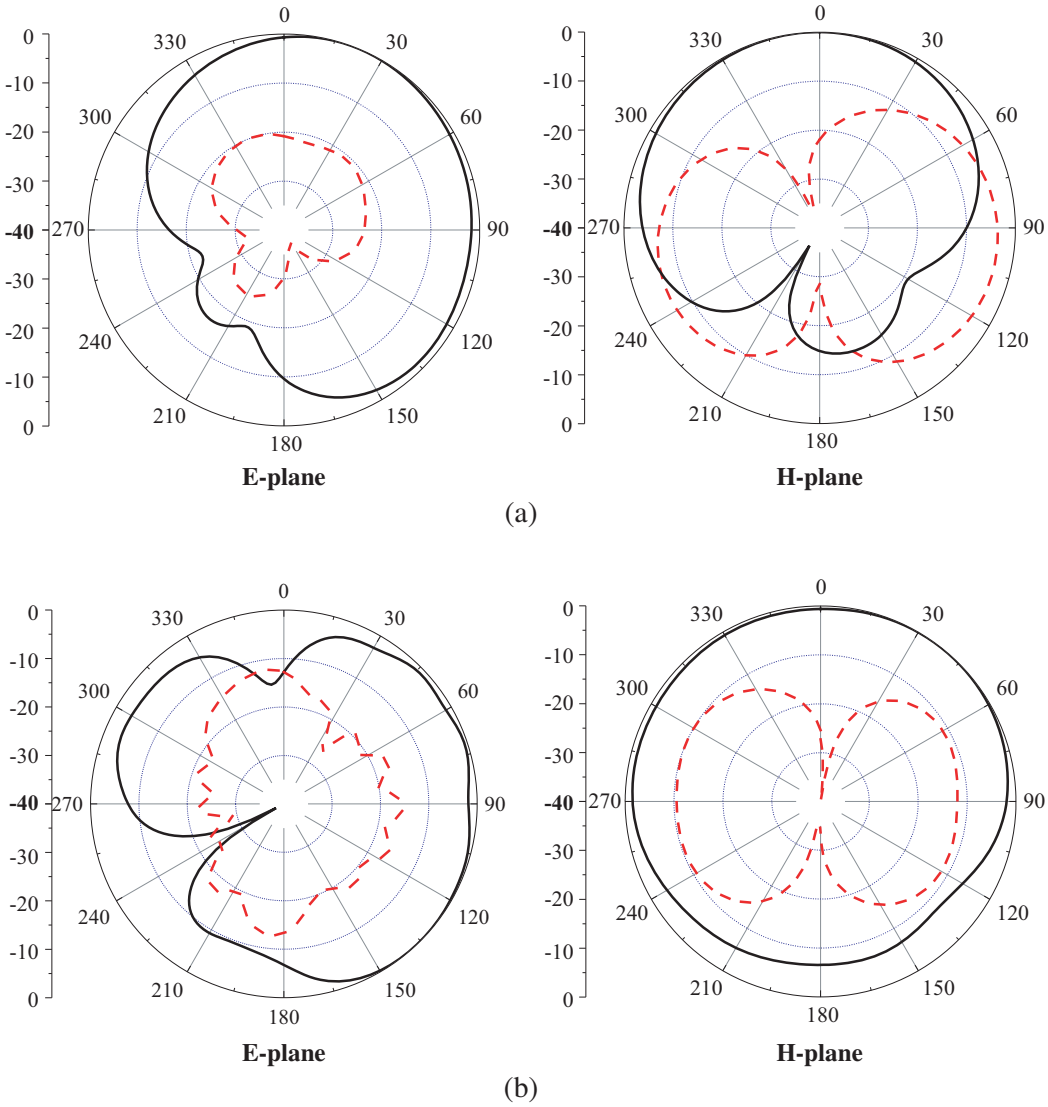

Figure 9. Radiation patterns of the proposed antenna. (a) 2.45 GHz. (b) 5.5 GHz.

The measured radiation patterns at 2.45 and 5.5 GHz for the proposed antenna are depicted in Figure 9. The co-pol and cross-pol are represented by solid and dot lines, respectively. The radiation patterns are measured in an anechoic chamber when one port (port 1) is excited and the other port (port 2) terminated by a 50-Ω load.

The envelope correlation coefficient (ECC) between antenna elements is one of the key parameters to evaluate the diversity performance of MIMO system, which takes mutual coupling into account. The S-parameter-based ECC can be obtained by [13]:

$$\rho_e = \frac{\left|S_{11}^* S_{12} + S_{21}^* S_{22}\right|^2}{\left(1 - |S_{11}|^2 - |S_{21}|^2\right)\left(1 - |S_{22}|^2 - |S_{12}|^2\right)} \tag{1}$$

Figure 10 illustrates the simulated and measured ECC curves of the proposed antenna. The measured ECC values are below 0.027 and 0.005 at the lower and higher operating frequency bands, respectively. Due to the smaller electrical distance separation, the ECC values at the lower frequency band are larger than those of the higher frequency bands. An ECC less than 0.5 is acceptable for wireless communication systems.

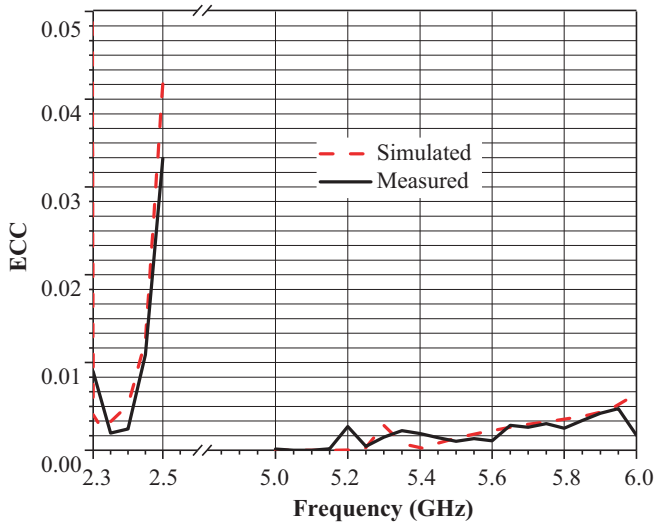

Figure 10. Simulated and measured ECC of the proposed antenna.

Table 2. Performance comparison with some published works.

Reference	−10 dB bandwidth (GHz)	Minimum Isolation (dB)	Peak Gain (dBi)	Overall size (mm^3)
[6]	2.4–2.5, 5.45–5.65	25, 15	1.8, 3	$19 \times 23 \times 0.8$
[7]	2.36–2.55, 5.52–5.83	20, 20	0.28, 3.88	$24 \times 25 \times 1.6$
[9]	2.2–2.7, 4.9–5.9	15	2.9, 4.5	$40 \times 40 \times 1.6$
[10]	3.2–3.8, 5.7–6.2	20	1.5, 2.8	$30 \times 26 \times 1.6$
[11]	5.7–5.93	20	5.45	$44.5 \times 77.5 \times 1.6$
[12]	2.46–2.7, 5.04–5.5	30	2.59, 3	$47.3 \times 74 \times 1.6$
This work	2.36–2.68, 4.81–5.95	24, 27	0.26, 3.1	$50 \times 30 \times 1.59$

The comparisons between the proposed antenna and the previous reported MIMO antennas are listed in Table 2. Compared with [9–12], the proposed antenna has a smaller size and higher isolation. Compared with [6, 7, 10], the proposed antenna shows larger bandwidth and higher isolation.

4. CONCLUSION

A novel multiband MIMO antenna is presented. The parasitic element and defected ground structure are experimentally shown to be effective in reducing mutual coupling and enhancing the radiation efficiency for the proposed MIMO antennas. The measured reflection coefficients, peak gains, and radiation patterns are presented. It is shown that the proposed antenna is a good candidate for IEEE 802.11 a/b/g/n frequency bands (2.4–2.5 GHz, 5.15–5.35 GHz, and 5.725–5.875 GHz) with high isolation and small ECC.

ACKNOWLEDGMENT

This work was supported in part by the National Natural Science Foundation of China under Grant Nos. 61340049 and 61671330, Science and Technology Department of Zhejiang Province under Grant No. LGG19F010009, and Wenzhou City Key Science and Technology Innovation Team Program under Grant No. C20170005.

REFERENCES

1. Ramachandran, A., S. Mathew, V. Rajan, and V. Kesavath, "A compact tri-band quad element MIMO antenna using SRR ring for high isolation," *IEEE Antennas & Wireless Propagation Letters*, Vol. 16, 1409–1412, 2017.
2. Lee, J. Y., J. Yeong, S. H. Kim, and J. H. Jang, "Reduction of mutual coupling in planar multiple antenna by using 1-D EBG and SRR structures," *IEEE Transactions on Antennas & Propagation*, Vol. 63, No. 9, 4194–4198, 2015.
3. Yang, Y. Y., Q. Chu, and C. Mao, "Multiband MIMO antenna for GSM, DCS, and LTE indoor applications," *IEEE Antennas & Wireless Propagation Letters*, Vol. 16, 1573–1576, 2016.
4. Zhang, S. and G. F. Pedersen, "Mutual coupling reduction for UWB MIMO antennas with a wideband neutralization line," *IEEE Antennas & Wireless Propagation Letters*, Vol. 15, 166–169, 2016.
5. Wang, S. and Z. Du, "Decoupled dual-antenna system using crossed neutralization lines for LTE/WWAN smartphone applications," *IEEE Antennas & Wireless Propagation Letters*, Vol. 14, 523–526, 2015.
6. Khan, M. S., M. F. Shafique, A. Naqvi, A.-D. Capobianco, B. Ijaz, and B. D. Braaten, "A miniaturized dual-band MIMO antenna for WLAN applications," *IEEE Antennas & Wireless Propagation Letters*, Vol. 14, 958–961, 2015.
7. Nandi, S. and A. Mohan, "A compact dual-band MIMO slot antenna for WLAN applications," *IEEE Antennas & Wireless Propagation Letters*, Vol. 16, 2457–2460, 2017.
8. Deng, J. Y., Z. J. Wang, J. Y. Li, and L. X. Guo, "A dual-band MIMO antenna decoupled by a meandering line resonator for WLAN applications," *Microw. Opt. Technol. Lett.*, Vol. 60, 759–765, 2018.
9. Liu, Y., Y. Lin, Y. Liu, J. Ren, J. Wang, and X. Li, "Dual-band planar MIMO antenna for WLAN application," *Microw. Opt. Technol. Lett.*, Vol. 57, 2257–2262, 2015.
10. Nirmal, P. C., A. B. Nandgaonkar, S. L. Nalbalwar, and R. K. Gupta, "A compact dual band MIMO antenna with improved isolation for Wi-Max and WLAN applications," *Progress In Electromagnetics Research M*, Vol. 68, 69–77, 2018.
11. Shahmirzadi, N. V. and H. Oraizi, "Design of reconfigurable coplanar waveguide-fed planar antenna for multiband multi-input-multi-output applications," *IET Microwaves Antennas & Propagation*, Vol. 10, 1591–1597, 2016.
12. Liu, P., D. Sun, P. Wang, and P. Gao, "Design of a dual-band MIMO antenna with high isolation for WLAN applications," *Progress In Electromagnetics Research Letters*, Vol. 74, 23–30, 2018.
13. Zhao, Y., F.-S. Zhang, L.-X. Cao, and D.-H. Li, "A compact dual band-notched MIMO diversity antenna for UWB wireless applications," *Progress In Electromagnetics Research C*, Vol. 89, 161–169, 2019.